First-principle studies of the lattice dynamics of crystals, and related properties

Xavier Gonze[*, I], Gian-Marco Rignanese[I] and Razvan Caracas[II]

[I] Université Catholique de Louvain, place Croix du sud 1, 1348 Louvain-la-Neuve Belgium
[II] Carnegie Institution of Washington, Geophysical Laboratory Broad Branch Rd., N.W. 5251 Washington DC 20015, USA

Abstract. The crystal lattice is never rigid. Due to temperature, external fields or pressure, the nuclei vibrate, the lattice distorts, and instabilities can induce phase transitions. We review the basic concepts of density-functional perturbation theory, a computational method especially suited to determine from first-principles the microscopic parameters governing such behaviour. Then, we present the additional formalism leading to the following properties of minerals: the infra-red and Raman spectra; the prediction of (meta)stability or instability of a crystalline phase, based on the phonon spectrum; the computation of thermodynamics quantities like the free energy, entropy, specific heat; the atomic temperature factors. For each property, examples are given. When appropriate, we mention the computation of related properties, like dielectric tensor and Born effective charges that are needed to get infra-red spectra. Finally, we discuss briefly, on one hand, other applications of the density-functional perturbation theory, and, on the other hand, an alternative technique, the finite-difference computation of dynamical matrices.

1. Introduction

The ability to investigate, from first-principles, properties of minerals for a static lattice at zero temperature, appears as an important step in crystallography and mineralogy. However, many effects, like phase transitions, infra-red or Raman spectra, require the ability to describe fluctuations of the nuclei positions with respect to their static equilibrium positions. The treatment of such effects, once the properties of the static lattice system are established, can be done in a coherent framework, treating small deformations by way of perturbation theory inside density functional theory (DFT) [1, 2]. The corresponding formalism, called density-functional perturbation theory (DFPT) [3–14] has been implemented in several computer programs

(see e.g. Refs. [15–23]). One of the goal of this review article will be to present enough of this formalism for the reader to be able to use such programs.

The application of this technique has already generated a large number of studies. In particular, the computation of selected vibrational frequencies, e.g. for comparison with infra-red and Raman data, is now routine, and can be performed for rather complicated crystal structures (e.g. see Ref. [24]). Although more involved, the computation of a full vibrational spectrum is an invaluable source of information on the behaviour of the crystal. It allows, inter alia, to determine whether a crystalline structure will present local instabilities, or, on the contrary, whether it is stable against all possible small deformations (e.g. see Ref. [25]). For high-pressure investigations, such predictions are crucial. The same vibrational spectrum will allow to deduce important thermodynamical data, like the temperature-dependent entropy, specific heat, internal energy or free energy, and give access to the atomic temperature factors, that are typical crystallographic experimental data.

For each property, we will deduce from the first-principles raw data, the specific quantities that can be linked to experimental results. Examples will be given for typical minerals, with special emphasis on oxides.

In section 2, we present the interatomic force constants and dynamical matrices, and emphasize that they are second-order derivatives of the energy. We present the vibrational spectrum of diamond. Such second-order derivatives can be computed within density-functional perturbation theory, described in section 3. In section 4, we focus on infra-red and Raman spectra, that are often complementary. In the same section, we examine the Born effective charges [26], and the associated quantity, the polarity of a vibrational mode. Zircon ($ZrSiO_4$) and barium titanate are taken as illustrative examples. The computation of the vibrational spectrum, and the prediction of instabilities will be the subject of section 5, illustrated with high-pressure $MgSiO_3$. Then, in section 6 and 7, we will present respectively the computation of thermodynamic quantities and the computation of atomic temperature factors, for which we will use SiO_2-quartz and SiO_2-stishovite as examples. We end with some discussion and perspectives.

---

* Correspondence author (e-mail: gonze@pcpm.ucl.ac.be)

2. Dynamical matrix and phonon frequencies

We consider a system of nuclei and electrons, in its electronic ground-state. In the framework of the Born-Oppenheimer (BO) approximation, the energy of such a system is a well-defined function of the position of the nuclei, that can be computed on the basis of density functional theory, or any many-body approach to the electronic structure problem. We will refer to this energy as the Born-Oppenheimer energy of the system, to which the kinetic energy of the nuclei should be added to obtain a total energy.

With respect to the periodic arrangement of nuclei, corresponding to the perfect classical crystal at zero temperature, small displacements around the equilibrium positions occur, and, in a classical viewpoint, evolve as a function of time. Such nuclear displacements induce changes in the BO energy, that can be expressed by a truncated second-order Taylor expansion, i.e. [14, 12]

$$E_{BO} = E_{BO}^{(0)} + \sum_{a\kappa\alpha} \sum_{b\kappa'\beta} \frac{1}{2} \left(\frac{\partial^2 E_{BO}}{\partial \tau_{\kappa\alpha}^a \, \partial \tau_{\kappa'\beta}^b} \right) \Delta\tau_{\kappa\alpha}^a \, \Delta\tau_{\kappa'\beta}^b \,, \tag{1}$$

where $\Delta\tau_{\kappa\alpha}^a$ is the displacement along direction α of the nucleus κ in the cell labeled a (with vector $\mathbf{R}_a$), from its equilibrium position τ_κ. When all displacements vanish, the BO energy is minimal, and is equal to $E_{BO}^{(0)}$. First-order derivatives vanish at the minimum, hence there are no linear terms in Eq. (1). The expansion of the BO energy truncated at second order is called the "harmonic approximation".

Forces and BO energies are related through the principle of virtual works: the force exerted on one nucleus in a specific direction is the opposite of the derivative of the BO energy due to an infinitesimal change of position of this nucleus along that direction. At the minimum of the BO energy, the forces vanish, in agreement with the first-order derivative of the energy being zero. When the nuclei are not at their equilibrium position, forces appear. In the harmonic approximation, they are linearly related to the displacement of every nucleus:

$$F_{\kappa\alpha}^a = -\sum_{b\kappa'\beta} \left(\frac{\partial^2 E_{BO}}{\partial \tau_{\kappa\alpha}^a \, \partial \tau_{\kappa'\beta}^b} \right) \Delta\tau_{\kappa'\beta}^b \,. \tag{2}$$

In order to describe the force on one nucleus, that arises because of the displacement of another nucleus (or of itself), in Eq. (2), one introduces the matrix of *interatomic force constants* (IFCs), defined as

$$C_{\kappa\alpha,\kappa'\beta}(a,b) = \left(\frac{\partial^2 E_{BO}}{\partial \tau_{\kappa\alpha}^a \, \partial \tau_{\kappa'\beta}^b} \right) \,. \tag{3}$$

The classical dynamics of the lattice is governed by Newton's law, giving the acceleration of each nucleus due to the forces acting upon it:

$$F_{\kappa\alpha}^a(t) = M_\kappa \frac{\partial^2 \tau_{\kappa\alpha}^a(t)}{\partial t^2} \,. \tag{4}$$

In the harmonic approximation, the general solutions of the evolution equation, Eq. (4), consist in a superposition of so-called normal modes of vibrations, labeled by the index σ, with amplitude a_σ (to be determined by initial conditions),

$$\Delta\tau_{\kappa\alpha}^a(t) = \sum_\sigma a_\sigma U_\sigma^a(\kappa\alpha) \, e^{i\omega_\sigma t} + (c.c) \,, \tag{5}$$

where the normal mode angular frequency, ω_σ, corresponds to a pattern of nuclear displacements $U_\sigma^a(\kappa\alpha)$. Both quantities are determined by the solution of a generalized eigenvalue equation, involving the interatomic force constants, as well as the masses of the nuclei

$$\sum_{\kappa'\beta b} C_{\kappa\alpha,\kappa'\beta}(a,b) \, U_\sigma^b(\kappa'\beta) = M_\kappa \omega_\sigma^2 U_\sigma^a(\kappa\alpha) \,. \tag{6}$$

Thanks to the periodicity of the lattice, and thus, the periodicity of the interatomic force constants (the interatomic force constants between equivalent pairs of nuclei related by the same translation are equal), the normal modes of vibrations can be characterized by a wavevector $\mathbf{q}$. They have the form of a Bloch wave, namely, the product of a wavevector-dependent phase factor, that varies from cell to cell, by a wavevector-dependent periodic function $U_{m\mathbf{q}}(\kappa\alpha)$:

$$U_\sigma^a(\kappa\alpha) = e^{i\mathbf{q}\cdot\mathbf{R}_a} U_{m\mathbf{q}}(\kappa\alpha) \,. \tag{7}$$

In the framework of quantum mechanics, such patterns of displacements are quantized and are called phonons. Note that in the right-hand side of Eq. (7) the index σ has been replaced by the composite index $m\mathbf{q}$, where the dependence on the wavevector appears explicitly.

Like the original pattern of displacement, the periodic part of the Bloch wave fulfills a generalized eigenvalue equation, compare with Eq. (6),

$$\sum_{\kappa'\beta} \tilde{C}_{\kappa\alpha,\kappa'\beta}(\mathbf{q}) \, U_{m\mathbf{q}}(\kappa'\beta) = M_\kappa \omega_{m\mathbf{q}}^2 U_{m\mathbf{q}}(\kappa\alpha) \,, \tag{8}$$

in term of the *dynamical matrices*, the Fourier transforms of the interatomic force constants

$$\tilde{C}_{\kappa\alpha,\kappa'\beta}(\mathbf{q}) = \sum_b C_{\kappa\alpha,\kappa'\beta}(0,b) \, e^{i\mathbf{q}\cdot\mathbf{R}_b} \,. \tag{9}$$

We normalize the eigendisplacements according to

$$\sum_{\kappa\alpha} M_\kappa [U_{m\mathbf{q}}(\kappa\alpha)]^* \, U_{m\mathbf{q}}(\kappa\alpha) = 1 \,. \tag{10}$$

The dynamical matrix, whose eigenvalues must be found, has dimension $3N_n \times 3N_n$, where N_n is the number of nuclei in the unit cell. Hence, there are $3N_n$ components in each eigenmode of displacement, as well as $3N_n$ distinct eigenmodes, corresponding to $3N_n$ eigenfrequencies (possibly degenerate), labeled by $m = 1 \dots 3N_n$.

The dispersion relations, giving the frequency of the phonons as a function of the wavevector $\mathbf{q}$, form "phonon bands". As for all waves propagating in a periodic medium, e.g. as electronic waves, the wavevectors are restricted in a portion of the reciprocal space, the Brillouin zone, whose boundaries are Bragg planes. Traditionally, the phonon dispersion relations are represented for a selected set of (high symmetry) lines in the Brillouin zone. As an example, we represent in Fig. 1 the phonon dispersion relations for diamond, as well as the corresponding Brillouin zone. Diamond has 2 nuclei per unit cell. Note
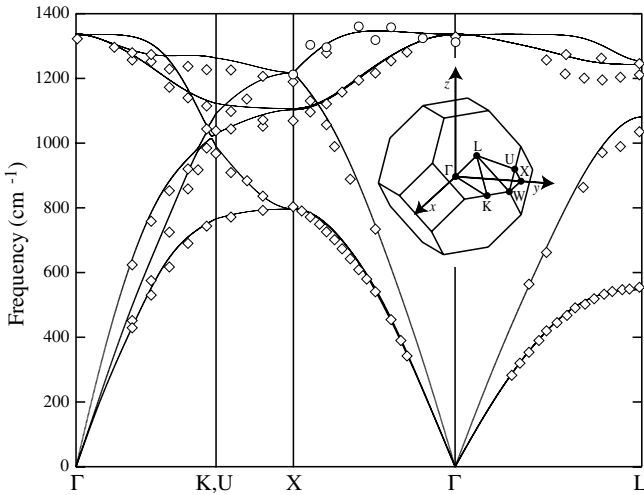
Fig. 1. Phonon dispersion relations for diamond. The frequencies are given in cm^{-1}. Experimental data are also indicated for comparison: the open diamonds have been obtained by neutron scattering [86] and the open circle (upper branch along the $\Gamma - X$ [100] direction) result from synchrotron scattering [87]. The corresponding Brillouin zone is also represented as an inset.

that the six phonon bands are clearly seen, along the Γ-K-X direction, where the possible degeneracies are lifted.

The Γ point, with $\mathbf{q} = (000)$, is the center of the Brillouin zone. Phonons with that wavevector have a pattern of displacement that is periodic (identical in all unit cells). By contrast, all the other points in the Brillouin zone correspond to waves with a phase varying from cell to cell, i.e. propagating waves. In Fig. 1, three phonon branches go to zero frequency when $\mathbf{q} \to \mathbf{0}$. They are called the acoustic branches. This effect is due to the translational invariance of the energy of the crystal. Such acoustic branches are found in all phonon spectra.

The computation of the dynamical matrix at one specific $\mathbf{q}$ wavevector is a routine task, if performed in the framework of DFPT (see next section). Still, it takes a non-negligible amount of computer time. Because of this, it is not a good strategy to perform band structure calculations, like for the one of diamond, based on hundreds of single $\mathbf{q}$ wavevector direct evaluations of dynamical matrices. Special techniques have been set up to interpolate the phonon dispersion relations throughout the whole Brillouin zone, from the knowledge of selected dynamical matrices. Such techniques, building upon the knowledge of asymptotic behaviour of the interatomic force constants, are based on Fourier transforms, and specific treatment of the dipole-dipole interaction. The interested reader might consult Refs. [7, 12] for more information about this.

The derivation of the existence and properties of the phonon band structure presented until now is purely classical. In quantum mechanics, at the level of the Born-Oppenheimer and harmonic approximations, the basic equations defining interatomic force constants, dynamical matrices, dispersion relations and Bloch waves are *exactly the same* as in classical mechanics. Still, the dynamics of the lattice cannot be described by Newton's law anymore, but by a many-body nuclear time-dependent wavefunction, related to the static ground-state by phonon creation operators. In the framework of this review, this difference with classical mechanics will have negligible consequences, except at the level of the computation of the phonon contribution to thermodynamical quantities or the atomic temperature factors. Interestingly, the differences can all be subsummed by the use of the Bose-Einstein statistical distribution, instead of the Maxwell-Boltzmann one. This will be the subject of Secs. 6 and 7.

In the following section, we will focus on DFPT, that allows the efficient computation of the second-order derivatives of the Born-Oppenheimer energy with respect to arbitrary nuclei displacement, needed to obtain the dynamical matrices, Eq. (9).

3. Density-functional perturbation theory

Density-functional perturbation theory focuses on the computation of the derivative of the DFT electronic energy with respect to different perturbations. This electronic energy is only a part of the Born-Oppenheimer energy: the nuclei-nuclei interaction energy must be added to it. However, the treatment of this additional contribution is much easier, because it involves only computing the electrostatic repulsion between classical point charges. See Ref. [12] for a complete treatment of this contribution.

The perturbations treated in DFPT might be external applied fields, as well as changes of potentials induced by nuclear displacements, or any type of perturbation of the equations that define the reference system. This powerful generic theory is able to deal with perturbations characterized by a non-zero, commensurate or incommensurate wavevector [27], with a workload similar to the one needed to deal with a periodic perturbation. Hence, it is particularly efficient for dealing with phonons. We first review briefly the DFT computation of the electronic energy, then proceeds with the computation of responses to perturbations. The description given here is far from complete. The interested reader will consult Refs. [11, 12, 14] for more information.

3.1 DFT equations

In the DFT [1, 2], we can derive the ground-state energy of the electronic system from the following minimum principle:

$$E_{\text{el}}\{\psi_\alpha\} = \sum_{\alpha}^{\text{occ}} \langle \psi_\alpha | \, T + v_{\text{ext}} \, | \psi_\alpha \rangle + E_{\text{Hxc}}[n] \,, \qquad (11)$$

where the ψ_α's are the Kohn-Sham orbitals (to be varied until the minimum is found), T is the kinetic energy operator, v_{ext} is the potential external to the electronic system, that includes the one created by nuclei, E_{Hxc} is the Hartree and exchange-correlation energy functional of the electronic density $n(\mathbf{r})$, and the summation runs over the occupied states α. For sake of simplicity, we do not treat varying occupation numbers, that would be needed for metals [10, 14], and consider only paramagnetic systems, with equal spin-up and spin-down densities.

The occupied Kohn-Sham orbitals are subject to the orthonormalization constraints,

$$\int \psi_\alpha^*(\mathbf{r}) \, \psi_\beta(\mathbf{r}) \, d\mathbf{r} = \langle \psi_\alpha | \psi_\beta \rangle = \delta_{\alpha\beta} \,, \qquad (12)$$

where α and β label occupied states (δ is Kronecker's symbol, 1 if $\alpha = \beta$, 0 otherwise). The density is generated from

$$n(\mathbf{r}) = \sum_{\alpha}^{\text{occ}} \psi_{\alpha}^{*}(\mathbf{r})\,\psi_{\alpha}(\mathbf{r})\,. \tag{13}$$

The minimization of $E_{\text{el}}\{\psi_{\alpha}\}$ under the orthonormality constraints Eq. (12) can be achieved using the Lagrange multiplier method. The problem turns into the minimization of

$$E_{\text{el}}^{+}\{\psi_{\alpha}\} = \sum_{\alpha}^{\text{occ}} \langle \psi_{\alpha} |\, T + v_{\text{ext}}\, | \psi_{\alpha} \rangle + E_{\text{Hxc}}[n]$$
$$- \sum_{\alpha\beta}^{\text{occ}} \epsilon_{\beta\alpha}\big(\langle \psi_{\alpha} \mid \psi_{\beta} \rangle - \delta_{\alpha\beta}\big)\,, \tag{14}$$

where $\epsilon_{\alpha\beta}$ are the Lagrange multipliers corresponding to the set of constraints Eq. (12). The canonical Euler-Lagrange equations are

$$H \,|\psi_{\alpha}\rangle = \sum_{\beta}^{\text{occ}} \epsilon_{\beta\alpha} \,|\psi_{\beta}\rangle\,, \tag{15}$$

where the Hamiltonian operator is

$$H = T + v_{\text{ext}} + \frac{\delta E_{\text{Hxc}}}{\delta n} = T + v_{\text{ext}} + v_{\text{Hxc}}\,. \tag{16}$$

Since H is Hermitian, it is always possible to make a unitary transformation of the wavefunctions in Eq. (15) in such a way that

$$H|\psi_{\alpha}\rangle = \epsilon_{\alpha}|\psi_{\alpha}\rangle\,. \tag{17}$$

In this way, we recover the usual Kohn-Sham equations.

3.2 Perturbation expansion

The DFT equations have been defined for generic external potentials v_{ext}. We now choose a reference (unperturbed) external potential $v_{\text{ext}}^{(0)}$ and expand the perturbed potential v_{ext} in terms of a small parameter λ, as follows, [4, 8]

$$v_{\text{ext}}(\lambda) = v_{\text{ext}}^{(0)} + \lambda v_{\text{ext}}^{(1)} + \lambda^{2} v_{\text{ext}}^{(2)} + \cdots\,. \tag{18}$$

We are interested in the change of physical quantities, due to the perturbation of the external potential [28]. So, we expand the different perturbed quantities $X(\lambda)$ using the same form as for $v_{\text{ext}}(\lambda)$,

$$X(\lambda) = X^{(0)} + \lambda X^{(1)} + \lambda^{2} X^{(2)} + \cdots\,, \tag{19}$$

where X can be the electronic energy E_{el}, the electronic wavefunctions $\psi_{\alpha}(\mathbf{r})$, the density $n(\mathbf{r})$, the electron eigenenergies $\epsilon_{\alpha\beta}$, or the Hamiltonian H. For example, the lowest-order expansion of Eq. (17) is simply

$$H^{(0)} \,|\psi_{\alpha}^{(0)}\rangle = \epsilon_{\alpha}^{(0)} \,|\psi_{\alpha}^{(0)}\rangle\,. \tag{20}$$

We suppose that all the zero-order quantities are known, as well as the change of external potential v_{ext} through all orders. In what follows, we suppose that the latter terms are the only applied perturbation, although the theory can be generalized to other forms of perturbation. For the computation of dynamical matrices, and other quantities presented in this review, only the first and second-order derivatives $v_{\text{ext}}^{(1)}$ and $v_{\text{ext}}^{(2)}$, are needed. Thus, we are looking

for the first-order changes of the wavefunctions, the density, the eigenenergies, as well as the first- and second-order changes of electronic energy. The DFPT allows to build them, as follows. We will not present the demonstrations of these DFPT equations, that fall outside of the scope of this review [3–5, 11].

Thanks to the variational property of the DFT electronic energy, the first-order derivative of the electronic energy can be evaluated without knowing any first-order quantity, except the change of external potential:

$$E_{\text{el}}^{(1)} = \sum_{\alpha}^{\text{occ}} \langle \psi_{\alpha}^{(0)} |\, v_{\text{ext}}^{(1)} \,| \psi_{\alpha}^{(0)} \rangle\,. \tag{21}$$

By contrast, the first-order change of wavefunctions, density, and Hamiltonian must be obtained self-consistently (or through a variational approach), in the same spirit as the self-consistent determination of the unperturbed wavefunctions, density and Hamiltonian. Indeed, supposing the first-order changes of wavefunctions $\psi_{\alpha}^{(1)}(\mathbf{r})$ are known, then, the first-order change of density can be obtained through [3]

$$n^{(1)}(\mathbf{r}) = \sum_{\alpha}^{\text{occ}} \psi_{\alpha}^{*(1)}(\mathbf{r})\,\psi_{\alpha}^{(0)}(\mathbf{r}) + \psi_{\alpha}^{*(0)}(\mathbf{r})\,\psi_{\alpha}^{(1)}(\mathbf{r})\,. \tag{22}$$

Knowing the first-order change of density, one can compute the first-order change of Hamiltonian $H^{(1)}$ thanks to [3]

$$H^{(1)} = v_{\text{ext}}^{(1)} + v_{\text{Hxc}}^{(1)}$$
$$= v_{\text{ext}}^{(1)} + \int \frac{\delta^{2} E_{\text{Hxc}}}{\delta n(\mathbf{r})\,\delta n(\mathbf{r}')}\bigg|_{n^{(0)}} n^{(1)}(\mathbf{r}')\,\mathrm{d}\mathbf{r}'\,. \tag{23}$$

Then, for the first-order wavefunctions, the self-consistent Sternheimer Eq. [11, 29], that depends on $H^{(1)}$ must be solved:

$$P_{c}(H^{(0)} - \epsilon_{\alpha}^{(0)})\, P_{c}\, |\psi_{\alpha}^{(1)}\rangle = -P_{c}H^{(1)}\, |\psi_{\alpha}^{(0)}\rangle\,, \tag{24}$$

where P_{c} is the projector upon the unoccupied states (conduction bands). As for the unperturbed quantities, powerful algorithms are available to solve the self-consistent cycle, Eqs. (22), (23), and (24).

For the second-order derivative of the electronic energy, different expressions can be used, whose ingredients are zero- and first-order quantities only. There is a simple non-variational expression

$$E_{\text{el}}^{(2)} = \sum_{\alpha}^{\text{occ}} \langle \psi_{\alpha}^{(0)} |\, v_{\text{ext}}^{(1)} \,| \psi_{\alpha}^{(1)} \rangle + \sum_{\alpha}^{\text{occ}} \langle \psi_{\alpha}^{(0)} |\, v_{\text{ext}}^{(2)} \,| \psi_{\alpha}^{(0)} \rangle\,, \tag{25}$$

or a more complex, and more accurate *variational* expression [5, 6, 11]:

$$E_{\text{el}}^{(2)}\{\psi^{(0)}; \psi^{(1)}\}$$
$$= \sum_{\alpha}^{\text{occ}} [\langle \psi_{\alpha}^{(1)} |\, H^{(0)} - \epsilon_{\alpha}^{(0)} \,| \psi_{\alpha}^{(1)} \rangle$$
$$+ (\langle \psi_{\alpha}^{(1)} |\, v_{\text{ext}}^{(1)} \,| \psi_{\alpha}^{(0)} \rangle + \langle \psi_{\alpha}^{(0)} |\, v_{\text{ext}}^{(1)} \,| \psi_{\alpha}^{(1)} \rangle)$$
$$+ \langle \psi_{\alpha}^{(0)} |\, v_{\text{ext}}^{(2)} \,| \psi_{\alpha}^{(0)} \rangle]$$
$$+ \frac{1}{2} \int\!\!\int \frac{\delta^{2} E_{\text{Hxc}}}{\delta n(\mathbf{r})\,\delta n(\mathbf{r}')}\bigg|_{n^{(0)}} n^{(1)}(\mathbf{r})\, n^{(1)}(\mathbf{r}')\,\mathrm{d}\mathbf{r}\,\mathrm{d}\mathbf{r}'\,, \tag{26}$$

where the first-order changes in wavefunctions $\psi_\alpha^{(1)}$ (these quantities will be referred to as the first-order wavefunctions, for brevity), can be varied under the constraints

$$\langle \psi_\alpha^{(0)} \mid \psi_\beta^{(1)} \rangle = 0 \,, \tag{27}$$

for all occupied states α and β. Since $E_{\rm el}^{(2)}\{\psi^{(0)}; \psi^{(1)}\}$ is variational with respect to $\psi^{(1)}$, one can deduce Euler-Lagrange equations, that turn out to be the self-consistent Sternheimer equation, Eq. (24).

This Sternheimer equation can be solved by algorithms based on Green's functions or, within some basis set, by standard algorithms for dealing with inhomogeneous systems of Eq. [14].

Except for symmetry breaking effects due to perturbations, the computer time needed to compute the self-consistent response to one perturbation is comparable to the computer time needed to compute the self-consistent ground-state properties of the crystalline system, at fixed nuclei positions.

3.3 Periodic systems: treatment of incommensurate perturbations

By Bloch's theorem, each wavefunction of a periodic system, whose external potential is left unchanged by a translation,

$$v_{\rm ext}^{(0)}(\mathbf{r} + \mathbf{R}_a) = v_{\rm ext}^{(0)}(\mathbf{r}) \,, \tag{28}$$

can be characterized by a wavevector $\mathbf{k}$, and written as a product of a phase factor by a *periodic function* $u_{m\mathbf{k}}^{(0)}$. Explicitly, for the ground-state wavefunctions,

$$\psi_{m\mathbf{k}}^{(0)}(\mathbf{r}) = (N_{\rm cell}\Omega_0)^{-1/2}\, e^{i\mathbf{k}\cdot\mathbf{r}}\, u_{m\mathbf{k}}^{(0)}(\mathbf{r}) \,, \tag{29}$$

where $N_{\rm cell}$ is the number of unit cells repeated in the Born-von Karman periodic box, and Ω_0 the volume of the unperturbed unit cell. m and $\mathbf{k}$ label the number of the electronic band and the wavevector of the wavefunction respectively. Eq. (29) is especially important: it is the key to the representation of the electronic system in the primitive unit cell, periodically repeated, instead of the full macroscopic space. The density is also periodic, and is obtained by performing an integral over the wavevectors in the whole Brillouin zone and summing on all the occupied bands:

$$n^{(0)}(\mathbf{r}) = \frac{1}{(2\pi)^3} \int\limits_{\rm BZ} \sum_m^{\rm occ} s u_{m\mathbf{k}}^{(0)*}(\mathbf{r})\, u_{m\mathbf{k}}^{(0)}(\mathbf{r})\, d\mathbf{k} \,, \tag{30}$$

where $s = 2$ is the spin factor (unlike in Eq. (13), both spin bands are taken into account in the summation over m).

We now investigate the form of the responses to perturbations characterized by a wavevector [4, 11, 45], namely, those with the following property (compare with Eq. (28)):

$$v_{\rm ext,\,\mathbf{q}}^{(1)}(\mathbf{r} + \mathbf{R}_a) = e^{i\mathbf{q}\cdot\mathbf{R}_a}\, v_{\rm ext,\,\mathbf{q}}^{(1)}(\mathbf{r}). \tag{31}$$

Applying a translation to the first-order wavefunctions and densities, the corresponding behaviours are

$$\psi_{m,\,\mathbf{k},\,\mathbf{q}}^{(1)}(\mathbf{r} + \mathbf{R}_a) = e^{i(\mathbf{k}+\mathbf{q})\cdot\mathbf{R}_a}\, \psi_{m,\,\mathbf{k},\,\mathbf{q}}^{(1)}(\mathbf{r}) \,, \tag{32}$$

and

$$n_{\mathbf{q}}^{(1)}(\mathbf{r} + \mathbf{R}_a) = e^{i\mathbf{q}\cdot\mathbf{R}_a}\, n_{\mathbf{q}}^{(1)}(\mathbf{r}) \,. \tag{33}$$

The factorization of the phase, in order to map the wave-vector-characterized (often incommensurate) problem to an equivalent one presenting the periodicity of the unperturbed problem is the crucial point in the treatment of perturbations like $v_{\rm ext,\,\mathbf{q}}^{(1)}$. For this purpose, inspired by Eqs. (32) and (33), one defines the *periodic* functions

$$u_{m,\,\mathbf{k},\,\mathbf{q}}^{(1)}(\mathbf{r}) = (N_{\rm cell}\Omega_0)^{1/2}\, e^{-i(\mathbf{k}+\mathbf{q})\cdot\mathbf{r}}\, \psi_{m,\,\mathbf{k},\,\mathbf{q}}^{(1)}(\mathbf{r}) \tag{34}$$

and

$$\bar{n}_{\mathbf{q}}^{(1)}(\mathbf{r}) = e^{-i\mathbf{q}\cdot\mathbf{r}}\, n_{\mathbf{q}}^{(1)}(\mathbf{r}) \,. \tag{35}$$

The periodic part of the first-order change in density is given by

$$\bar{n}_{\mathbf{q}}^{(1)}(\mathbf{r}) = \frac{2}{(2\pi)^3} \int\limits_{\rm BZ} \sum_m^{\rm occ} s u_{m\mathbf{k}}^{(0)*}(\mathbf{r})\, u_{m\mathbf{k},\,\mathbf{q}}^{(1)}(\mathbf{r})\, d\mathbf{k} \,. \tag{36}$$

In the same spirit, the factorization of the phase can also be accomplished at the level of Sternheimer equation. As a final result, all the first-order quantities can be obtained by solving equations in which the translational symmetry has been restored, that is, all the basic quantities to be determined are periodic.

3.4 Response to an homogeneous, static electric field

For the computation of the infra-red response, one must treat not only changes in the potential due to the collective nuclei displacements, but also changes associated with an homogeneous, low-frequency electric field (low-frequency compared to the typical electronic excitation energy). Two important problems arise when one attempts to deal with the response to such an electric field $\mathcal{E}_{\rm mac}$. The first problem comes from the fact that the potential energy of the electron, placed in such a field, is linear in space, and breaks the periodicity of the crystalline lattice:

$$v_{\rm scr}(\mathbf{r}) = \sum_\alpha \mathcal{E}_{{\rm mac},\,\alpha} r_\alpha \,. \tag{37}$$

Second, this macroscopic electric field corresponds to a screened potential: the change of macroscopic electric field is the sum of an external change of field and an internal change of field, the latter being induced by the response of the electrons (the polarization of the material). In order to indicate this fact, the subscript "scr" has been used in Eq. (37). In the theory of classical electromagnetism, one writes the connection between the macroscopic displacement, electric and polarization fields as

$$\mathcal{D}_{\rm mac}(\mathbf{r}) = \mathcal{E}_{\rm mac}(\mathbf{r}) + 4\pi\mathcal{P}_{\rm mac}(\mathbf{r}) \,, \tag{38}$$

where $\mathcal{P}_{\rm mac}(\mathbf{r})$ is related to the macroscopic charge density by

$$n_{\rm mac}(\mathbf{r}) = -\nabla \cdot \mathcal{P}_{\rm mac}(\mathbf{r}) \,. \tag{39}$$

The long-wave method is commonly used to deal with the first problem: a potential linear in space is obtained as

the limit for $\mathbf{q}$ tending to $\mathbf{0}$ of

$$v(\mathbf{r}) = \lim_{\mathbf{q} \to \mathbf{0}} \lambda \, \frac{2 \sin \mathbf{q} \cdot \mathbf{r}}{|\mathbf{q}|} = \lim_{\mathbf{q} \to \mathbf{0}} \lambda \left(\frac{e^{i\mathbf{q} \cdot \mathbf{r}}}{i|\mathbf{q}|} - \frac{e^{-i\mathbf{q} \cdot \mathbf{r}}}{i|\mathbf{q}|} \right),$$

(40)

where $\mathbf{q}$ is in the direction of the homogeneous field. The detailed theoretical treatment of the response to an electric field, using the long-wave method, and treating the screening adequately (in order to solve the above-mentioned second problem) is given in Ref. [12]. It is found that an auxiliary quantity is needed: the derivative of the ground-state wavefunctions with respect to their wavevector. Interestingly, this quantity, being a derivative, can also be computed within DFPT. Once this quantity has been obtained, the computation of the response to an homogeneous electric field *per se* can be performed, also within DFPT.

3.5 Derivatives of the electronic energy with respect to mixed perturbations

Until now, we have focused on one perturbation of the system, and the corresponding first- and second-order derivatives. However, the dynamical matrices or interatomic force constants are *mixed* second-order derivatives of the Born-Oppenheimer energy, corresponding to two different (groups of) nuclear displacements. Also, we will need mixed derivatives of the energy with respect to atomic displacements and an homogeneous electric field, in order to obtain the coupling between phonon and electric field.

DFPT is able to deal straightforwardly with such mixed derivatives. We consider two or more simultaneous Hermitian perturbations, combined in a Taylor-like expansion of the following type (see Ref. [4, 12] for the notation):

$$v_{\text{ext}}(\boldsymbol{\lambda}) = v_{\text{ext}}^{(0)} + \sum_{j_1} \lambda_{j_1} v_{\text{ext}}^{j_1} + \sum_{j_1 j_2} \lambda_{j_1} \lambda_{j_2} v_{\text{ext}}^{j_1 j_2} + \cdots \quad (41)$$

(the indices j_1 and j_2 are not exponents, but label the different perturbations). The mixed derivative of the energy of the electronic system

$$E_{\text{el}}^{j_1 j_2} = \frac{1}{2} \frac{\partial^2 E_{\text{el}}}{\partial \lambda_{j_1} \, \partial \lambda_{j_2}} \quad (42)$$

is obtained from the simple expression

$$E_{\text{el}}^{j_1 j_2} = \sum_{\alpha}^{\text{occ}} \langle \psi_{\alpha}^{j_2} | \, v_{\text{ext}}^{j_1} \, | \psi_{\alpha}^{(0)} \rangle + \sum_{\alpha}^{\text{occ}} \langle \psi_{\alpha}^{(0)} | \, v_{\text{ext}}^{j_1 j_2} \, | \psi_{\alpha}^{(0)} \rangle. \quad (43)$$

In the expression Eq. (43), the first-order derivative of the wavefunctions with respect to the first perturbation $| \psi_{\alpha}^{j_1} \rangle$ are not needed, while the computation of $v_{\text{ext}}^{j_1}$ and $\langle \psi_{\alpha}^{(0)} | \, v_{\text{ext}}^{j_1 j_2} \, | \psi_{\alpha}^{(0)} \rangle$ takes little time. Similar expressions, that do not involve $| \psi_{\alpha}^{j_2} \rangle$ but $| \psi_{\alpha}^{j_1} \rangle$ are also available, as well as more accurate stationary expressions.

Thus, the ability to compute the first-order responses (i.e., changes in wavefunctions and densities) to the basic perturbations described previously gives us also, as by-products, mixed second-order derivatives of the electronic energy. Actually, even third-order mixed derivatives of the energy might be computed straightforwardly, thanks to the $2n + 1$ theorem of perturbation theory, within DFPT [4].

We will not present the corresponding formalism, but only briefly mention some of its applications, in Sec. 8.

We are now in a position to examine selected properties of minerals, that can be computed thanks to the present formalism.

4. Infra-red and Raman spectra

Electromagnetic (EM) radiation, or photons (in quantum theory) interact in several ways with a mineral. For an insulating solid, and considering EM frequencies in the infra-red range, phonons are the predominant cause of features in the absorption or reflection spectra.

Only phonons with a very small wavevector $\mathbf{q} \approx 0$ interact with photons. Indeed, the photons absorbed and emitted should have an energy comparable to the one of phonons, that is, 0.3 eV at most. Such photons have a very large wavelength (larger than 3 μm), compared to the typical unit cell size, hence a very small wavevector. Even in the case of scattering of photons of higher energies (e.g. the Raman scattering, with photon energies around a few eV), the involved phonons all have negligible wavevectors.

For this $\mathbf{q} \approx 0$ limit, symmetry considerations, formalized in the framework of group theory, allow to classify the phonons according to the irreducible representations of the crystal point group. We refer to standard textbooks (e.g. see Ref. [30]) for a detailed explanation of these concepts. In particular, for crystals possessing a center of inversion, there will be representations invariant with respect to inversion ("gerade" or "g" modes), as well as representations associated with phonon modes whose eigendisplacement pattern changes sign under inversion ("ungerade" or "u" modes). Further classification will examine the behaviour of phonon modes under other symmetry operations. Beyond phonon modes, many properties of crystals, like dielectric tensors, elastic constants, thermal expansion coefficients, spontaneous polarization, might be classified according to irreducible representations. Group theory allows to deduce transformation laws of these objects, and even predict the vanishing of some effects, or selected components of the response tensors. For example, in the case of the spontaneous polarization (a vector), one should examine the way a vector transforms under the operations of the point group. In particular, a vector always changes signs under inversion, hence a crystal with inversion symmetry cannot have a spontaneous polarization.

Two experimental techniques are commonly used for phonon spectroscopy with EM fields: intra-red reflectivity (or absorption), and Raman scattering. They are quite complementary, because the involved phonon often belongs to different irreducible representations. We first focus on the infra-red reflectivity.

4.1 Infra-red spectrum

The reflectivity of EM waves normal to the surface, having their electric field with direction $\mathbf{q}$ along an optical axis of the crystal, is given in terms of the frequency-de-

pendent dielectric permittivity $\epsilon_{\hat{\mathbf{q}}}$:

$$R(\omega) = \left| \frac{\epsilon_{\hat{\mathbf{q}}}^{1/2}(\omega) - 1}{\epsilon_{\hat{\mathbf{q}}}^{1/2}(\omega) + 1} \right|^2 . \qquad (44)$$

More general expressions for the reflectivity, or for the absorption, may be found in classical textbooks [31]. The dielectric permittivity along direction $\hat{\mathbf{q}}$ is computed from the dielectric permittivity tensor

$$\epsilon_{\hat{\mathbf{q}}}(\omega) = \sum_{\alpha\beta} \hat{q}_\alpha \epsilon_{\alpha\beta}(\omega) \hat{q}_\beta . \qquad (45)$$

Let us examine the first-principle approach to this tensor. In the infra-red frequency regime, the dielectric permittivity tensor obtained in the harmonic approximation can be split in two parts, the electronic contribution $\epsilon_{\alpha\beta}^\infty$, taken as frequency independent, and the phonon contribution. We describe now the coupling between phonons and an homogeneous electric field.

There are two connected effects: forces created by an applied electric field, and polarization created by nuclear displacements. The Born effective charge tensor $Z_{\kappa,\beta\alpha}^*$ is defined as the proportionality coefficient relating, at linear order, the polarization per unit cell created along the direction β, to the displacement along the direction α of the nuclei belonging to the sublattice κ, under the condition of zero electric field [3, 12, 26]. The same coefficient also describes the linear relation between the force on a nucleus and the macroscopic electric field, because both effects can be connected to the mixed second-order derivative of the energy with respect to nuclei displacements and macroscopic electric field:

$$Z_{\kappa,\beta\alpha}^* = \Omega_0 \frac{\partial \mathcal{P}_{\mathrm{mac},\beta}}{\partial \tau_{\kappa\alpha}(\mathbf{q}=\mathbf{0})} = \frac{\partial F_{\kappa,\alpha}}{\partial \mathcal{E}_\beta} = -\frac{\partial E_{\mathrm{BO}}}{\partial \mathcal{E}_\beta \, \partial \tau_{\kappa\alpha}(\mathbf{q}=\mathbf{0})} . \qquad (46)$$

The Born effective charge tensors fulfill an important sum rule stemming from the fact that a global translation of a neutral crystal, as a whole, should not change its polarization. This sum rule implies that the charge neutrality is fulfilled at the level of the Born effective charges. For every directions α and β, one must have [32]:

$$\sum_\kappa Z_{\kappa,\alpha\beta}^* = 0 , \qquad (47)$$

i.e., the sum of the Born effective charges of all nuclei in one cell must vanish, element by element. In DFT computations, this sum rule will be broken because of the incompleteness of the basis set used to represent wave functions, because of the discreteness of special point grids, or because of the discretization of the real space integral (needed for the evaluation of the exchange-correlation energies and potentials). Techniques to reinstall the Born effective charge neutrality sum rule are described in Ref. [12].

The knowledge of Born effective charge tensors for each nuclei, and the eigenvectors of the dynamical matrix at the Brillouin zone center, is sufficient to describe fully the photon-phonon interaction in the harmonic approximation. Following Ref. [33], the quantity

$$p_{m\alpha} = \sum_{\kappa\beta} Z_{\kappa,\alpha\beta}^* U_{m\mathbf{q}=\mathbf{0}}(\kappa\beta) , \qquad (48)$$

that combines Born effective charges with the phonon eigendisplacements, is referred to as the *polarity* of the phonon mode m. The three components $p_{m\alpha}$ form a vector $\mathbf{p}_m$, whose sign is arbitrary (Eq. (10) leaves the sign of the eigendisplacement vector unspecified) [34]. In term of mode polarities, the dielectric tensor $\epsilon_{\alpha\beta}(\omega)$ has a rather simple expression:

$$\epsilon_{\alpha\beta}(\omega) = \epsilon_{\alpha\beta}^\infty + \frac{4\pi}{\Omega_0} \sum_m \frac{p_{m\alpha} p_{m\beta}}{\omega_m^2 - \omega^2} , \qquad (49)$$

and the dielectric permittivity along some direction $\hat{\mathbf{q}}$, Eq. (45), becomes

$$\epsilon_{\hat{\mathbf{q}}}(\omega) = \sum_{\alpha\beta} \hat{q}_\alpha \epsilon_{\alpha\beta}^\infty \hat{q}_\beta + \frac{4\pi}{\Omega_0} \sum_m \frac{(\mathbf{p}_m \cdot \mathbf{q})^2}{\omega_m^2 - \omega^2} . \qquad (50)$$

Equations (49) and (50) express $\epsilon_{\alpha\beta}(\omega)$ and $\epsilon_{\hat{\mathbf{q}}}(\omega)$ as coming from an electronic contribution $\epsilon_{\alpha\beta}^\infty$ (approximated as frequency-independent in the IR regime), and contributions from each possible phonon mode m at the Brillouin zone center. The phonon contributions have a characteristic frequency dependence: there is a resonant behaviour when the frequency of light matches the one of a phonon, in which case the denominator of Eq. (50) vanishes. The latter equation shows that, if the vector $\mathbf{p}_m$ is perpendicular to $\mathbf{q}$, the direction of the electric field, the mode m does not contribute to the dielectric permittivity constant along $\mathbf{q}$. For each mode m, there will thus be one direction along which the mode contributes to the dielectric permittivity constant, in which case it is referred to as longitudinal, while for the perpendicular directions, the mode will be referred to as transverse. In this way, we find the (well-known) distinction between the longitudinal optic (LO) modes and the transverse optic (TO) modes. This distinction will be the subject of further explanation later.

Alternatively, the same value of the dielectric permittivity tensor might be obtained in terms of the Born effective charge tensors and the zone-center dynamical matrix, see Eq. (52) of Ref. [11], from which one deduces the following expression of the static $\omega = 0$ dielectric permittivity tensor,

$$\epsilon_{\alpha\beta}^0 = \epsilon_{\alpha\beta}^\infty + \frac{4\pi}{\Omega_0} \sum_{\kappa\kappa'} \sum_{\alpha'\beta'}$$

$$\times \left(Z_{\kappa,\alpha\alpha'}^* \left[\tilde{C}(\mathbf{q}=\mathbf{0}) \right]_{\kappa\alpha',\kappa'\beta'}^{-1} Z_{\kappa',\beta\beta'}^* \right) . \qquad (51)$$

This equation highlights that, when the frequency is sufficiently small as to allow nuclei to relax to their equilibrium position under the applied field, their masses do not play a role anymore: the static $\omega = 0$ dielectric permittivity tensor is independent of the masses.

As an application of this theory we examine the case of barium titanate. $BaTiO_3$ crystallizes in the perovskite structure (with one formula unit per cell). Above 130 °C, it is cubic, and undergoes three phase transitions when the temperature is lowered, with slight departure of the nuclei positions from their reference ones, accompanied by small lattice vector changes, reaching a rhombohedral structure around −90 °C. Figure 2 presents the theoretical reflectivity spectrum of rhombohedral $BaTiO_3$ [35], following Eq. (44). Experimental results for the cubic phase have been obtained in Ref. [36]. The major experimental trends are
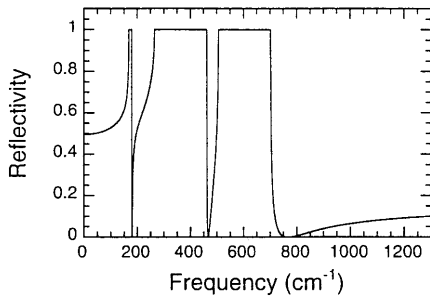
Fig. 2. Infra-red reflectivity of rhombohedral BaTiO$_3$, with $\hat{\mathbf{q}}$ along the ferroelectric direction. Reprinted from Ref. [35].

reproduced by the theory. The characteristic frequencies of the spectrum (minima and plateaus) directly related to phonon frequencies at the Brillouin zone center, agree with those of the experiment. However, there are noticeable differences. In particular, the experimental reflectivity never reaches 100%, it is always lower than about 85%. Such an effect is due to the damping of phonon modes, absent in the theoretical treatment (e.g. the phonon-phonon interaction is neglected in the harmonic theory).

Let us come back to the distinction between LO and TO modes. When a phonon interact with an electric field, it can do so even if the electric field is internal (it does not interact only with applied electric fields, but also with electric fields that were induced by itself). This phenomenon is seen in the analysis of the limiting behaviour of the dynamical matrix in the long wavelength $\mathbf{q} \to 0$ limit [12, 14]. The dynamical matrix $\tilde{C}_{\kappa\alpha,\kappa'\beta}(\mathbf{q} \to 0)$ can be split in two parts, one that behaves smoothly as a function of the wavevector, $\tilde{C}_{\kappa\alpha,\kappa'\beta}(\mathbf{q} = \mathbf{0})$, and one that will vary according to the direction of the $\mathbf{q} \to 0$ limit:

$$\tilde{C}_{\kappa\alpha,\kappa'\beta}(\mathbf{q} \to \mathbf{0}) = \tilde{C}_{\kappa\alpha,\kappa'\beta}(\mathbf{q} = \mathbf{0}) + \tilde{C}_{\kappa\alpha,\kappa'\beta}^{\text{NA}}(\mathbf{q} \to \mathbf{0}) \,. \tag{52}$$

The non-analytical, direction-dependent term $\tilde{C}_{\kappa\alpha,\kappa'\beta}^{\text{NA}}(\mathbf{q} \to \mathbf{0})$ is given by

$$\frac{4\pi}{\Omega_0} \frac{\left(\sum_\gamma q_\gamma Z_{\kappa,\gamma\alpha}^*\right)\left(\sum_{\gamma'} q_{\gamma'} Z_{\kappa',\gamma'\beta}^*\right)}{\sum_{\alpha\beta} q_\alpha \epsilon_{\alpha\beta}^\infty q_\beta} \,. \tag{53}$$

In general, the eigenvectors of the $\tilde{C}(\mathbf{q} \to 0)$ matrix will not be identical to those of the $\tilde{C}(\mathbf{q} = \mathbf{0})$. However, the modes that have a polarity vector $\mathbf{p}_m$ perpendicular to the direction of $\mathbf{q}$ are common to both, and are called transverse optic for that direction of $\mathbf{q}$. Indeed, the non-analytical term in Eq. (52) does not modify the eigenfrequency of displacement vectors $U_{m\mathbf{q}=\mathbf{0}}(\kappa'\beta)$ for which

$$\sum_{\kappa'\beta} \left(\sum_{\gamma'} q_{\gamma'} Z_{\kappa',\gamma'\beta}^*\right) U_{m\mathbf{q}=\mathbf{0}}(\kappa'\beta) = \mathbf{q} \cdot \mathbf{p}_m = 0 \,. \tag{54}$$

All the others modes, that are changed because they couple to the electro-magnetic field that they induce, will be called longitudinal optic for that direction of $\mathbf{q}$. It is important to emphasize that the LO-TO splitting is a directional effect: considering a $\mathbf{q} = 0$ mode (at the Brillouin zone center), with a given non-zero polarity vector, there will be a plane of $\mathbf{q}$ vectors perpendicular to $\mathbf{p}_m$ leaving

the frequency and eigendisplacements unaffected, while the latter will change if the limiting direction is different.

For selected systems, symmetry constraints will be sufficient to guarantee that some LO eigendisplacements of $\tilde{C}(\mathbf{q} \to 0)$ will be identical to those of $\tilde{C}(\mathbf{q} = 0)$, even if the eigenfrequencies are not the same. In this case, the following relation, linking LO and TO modes, holds:

$$\omega_m^2(\mathbf{q} \to \mathbf{0}) = \omega_m^2(\mathbf{q} = \mathbf{0}) + \left(\frac{4\pi}{\Omega_0}\right) \frac{(\mathbf{q} \cdot \mathbf{p}_m)^2}{\sum_{\alpha\beta} q_\alpha \epsilon_{\alpha\beta}^\infty q_\beta} \,. \tag{55}$$

In general, symmetry considerations will be very important to understand the IR spectrum. Only the phonon modes belonging to irreducible representations that transform like a vector, or the components of a vector, will couple with an electric field. This is because the coupling between the electric field and the phonon is described by the polarity of the mode, a vector, and this vector will vanish for all phonons belonging to an irreducible representation that is incompatible with the behaviour of a vector. In particular, for centro-symmetric materials, only the ungerade (u) modes interact with an electric field. This also holds for the interaction with the internal long-wavelength electric field. Phonons belonging only to selected irreducible representations will exhibit a LO-TO splitting.

4.2 Raman spectrum

In a Raman experiment, the (polarized) incident light is scattered by the sample, and the energy as well as polarization of the outgoing light is measured. A Raman spectrum, presenting the energy of the outgoing photons, will consist of rather well-defined peaks, around an elastic peak (corresponding to outgoing photons that have the energy of the incident photons).

At the lowest order of the theory, the dominant mechanism is the absorption or emission of a phonon by a photon. A measure of the energy difference between the outgoing and incident photons gives the energy of the absorbed or emitted phonon. Thus, even more straightforwardly than the IR spectrum, a Raman spectrum relates to the energy of phonons at the Brillouin-zone center: when the zero of the frequency scale is set at the incident light frequency, the absolute value of the energy of the peaks corresponds to the energy of the phonons.

However, the coupling between a phonon and a photon, in a Raman process, is not described by the Born effective charges, but by the Raman efficiency $\alpha_{\beta\gamma}^m$, linked to the change of the electronic linear dielectric susceptibility tensor χ due to the collective displacement of nuclei corresponding to the phonon mode [33, 67, 70]:

$$\alpha_{\beta\gamma}^m = \sqrt{\Omega_0} \sum_{\kappa\delta} \frac{\partial \chi_{\beta\gamma}^{(1)}}{\partial \tau_{\kappa\delta}} U_{m\mathbf{q}=\mathbf{0}}(\kappa\delta) \,. \tag{56}$$

Such a mechanism does not appear at the level of the harmonic approximation. It is the change of a linear response coefficient (the susceptibility tensor) due to a phonon. As such, it can be linked to a third-order derivative of the energy. The DFPT can be extended to handle such third-order derivatives of the energy, as mentioned previously.

This formalism has been implemented, but the computations of Raman efficiencies are still quite scarce, see Sec. 8. This situation might change in the future. By contrast, the computation of phonon frequencies, and their comparison with the data provided by the Raman spectrum, without taking into account the Raman efficiencies, is rather common and instructive.

This comparison is helped by the fact that one can predict the vanishing of many Raman efficiencies on the basis of group theory. Indeed, for a Raman efficiency to be non-zero, the corresponding phonon mode must transform like a scalar, or a second-order symmetric tensor, or any component thereof. Examination of irreducible representations, and their compatibility with such quantities will readily allow to determine which classes of phonons will scatter light in a Raman experiment. In particular, in the case of a centro-symmetric crystal, a phonon must be invariant under inversion symmetry ("gerade"), in order to have non-vanishing Raman efficiency. This result is the opposite of what is found for the infra-red spectroscopy. Thus, for centro-symmetric crystals, a phonon mode cannot be both infra-red and Raman active. Quite understandably, these two experimental techniques often prove to be complementary. However, not all phonons are either infra-red or Raman active. For selected point groups, there are some irreducible representations that are neither compatible with a scalar, or a vector, or a symmetric tensor behaviour. The phonons belonging to such classes are called "silent".

4.3 An example: zircon

Zircon ($ZrSiO_4$) has a conventional unit cell which is body-centered tetragonal (space group $I4_1/amd$, N° 141) and contains four formula units of $ZrSiO_4$. A primitive cell containing only two formula units can be defined. The structure of zircon may be viewed as consisting of $(SiO_4)^{4-}$ anions and Zr^{4+} cations, as illustrated in Fig. 1 of Ref. [37]. We present now the zircon phonon frequencies at the Brillouin zone center, from Ref. [38].

In Table 1, the calculated phonon frequencies are compared with experimental values [37, 39, 40]. Overall, the agreement is excellent, with a rms absolute deviation of 9.4 cm^{-1}, and a *rms* relative deviation of 2.5%. Two Raman active modes are obtained at 631.7 cm^{-1} [$B_{1g}(3)$] and at 922.6 cm^{-1} [$E_g(5)$], that could not be detected experimentally. Silent modes, inactive for both IR and Raman experiments, are also observed. They are found to range from 119.6 to 943.3 cm^{-1}. Two of these (B_{1u} and A_{2g}) are very soft, and correspond, in a first approximation, to vibration modes of zircon in which the SiO_4 tetrahedra rotate as a unit [37].

On the basis of the close correspondence between these results and experimental data for IR-active and Raman-active modes, one is able to shed light on some delicate issues related to the interpretation of experimental results and the corresponding symmetry assignment.

Indeed, these calculations do not give any frequency of E_g symmetry close to the frequency of 1008 cm^{-1} experimentally observed by Dawson et al. [37]. This lends support to their interpretation, which suggested that this line does not result from the perfect crystal, but rather from some crystal misorientation or imperfection. By contrast,

Table 1. Fundamental frequencies of zircon (in cm^{-1}) with their symmetry assignments. The experimental values are taken from Ref. [37] (first experimental data column), Ref. [39] (for A_{2u} mode in the second experimental data column), and Ref. [40] (for E_u mode in the second experimental data column).

Mode	This work	Experiment	
Raman			
$A_{1g}(1)$	442.0	439	
$A_{1g}(2)$	971.4	974	
$B_{1g}(1)$	225.4	214	
$B_{1g}(2)$	396.9	393	
$B_{1g}(3)$	631.7	–	
$B_{1g}(4)$	1016.7	1008	
B_{2g}	251.8	266	
$E_g(1)$	194.3	201	
$E_g(2)$	224.7	225	
$E_g(3)$	375.4	357	
$E_g(4)$	536.0	547	
$E_g(5)$	922.6	–	
Infra-red			
A_{2u} (TO1)	347.8	338	339
A_{2u} (LO1)	475.9	480	478
A_{2u} (TO2)	601.2	608	605.7
A_{2u} (LO2)	646.0	647	641.5
A_{2u} (TO3)	979.9	989	977
A_{2u} (LO3)	1096.2	1108	1100
E_u (TO1)	285.2	287	281
E_u (LO1)	340.6	352	354
E_u (TO2)	383.0	389	381
E_u (LO2)	420.2	419	417
E_u (TO3)	422.2	430	429
E_u (LO3)	466.4	471	468
E_u (TO4)	867.4	885	871
E_u (LO4)	1028.6	1035	1034
Silent			
B_{1u}	119.6	–	
A_{2g}	241.7	–	
A_{1u}	392.3	–	
$B_{2u}(1)$	566.4	–	
$B_{2u}(2)$	943.3	–	

as mentioned previously, an E_g mode can be identified at 922.6 cm^{-1}.

Furthermore, one can propose that the weak band found in experiments at 547 cm^{-1} should not be interpreted as a difference band between lines at 989 cm^{-1} (A_{2u} symmetry) and at 439 cm^{-1} (A_{1g} symmetry) [37], but rather as the frequency of a real eigenmode. In fact, a phonon frequency of E_g symmetry is found at 536 cm^{-1}, quite close to this weak band (547 cm^{-1}). This reassignment has been taken into account in Table 1.

5. Instabilities predicted by phonon band structures

The availability of the phonon band structure in the whole Brillouin zone for a crystalline phase allows to determine

the (meta) stability of this phase, that is, its stability with respect to any possible small distortion of the crystal structure.

Indeed, let us suppose that one has determined a structure for which the forces on all nuclei vanish. In the case there is a pattern of displacements that does not experience a restoring force towards the structure under investigation, but on the contrary, a force that amplifies it, the change of energy, at second order, described by Eq. (1), will be negative. Thus, the matrix of interatomic force constants will not be definite-positive. There will be some eigenmode of Eq. (6) associated with a negative value of ω_σ^2 (the corresponding eigenfrequency ω_σ is imaginary). Furthermore, the Bloch analysis is still valid, and an imaginary eigenfrequency should also be seen in Eq. (9).

A contrario, if all the eigenfrequencies of the phonon band structure are real, any pattern of displacements, with a sufficiently small amplitude, will always raise the energy, and will feel a restoring force towards the starting configuration.

Figure 3 presents an example of a crystal where an instability is identified in the phonon band structure. In part (a) the ideal cubic phase of $MgSiO_3$ perovskite, the major component of the Earth's lower mantle, presents several unstable phonon modes. Along the X-M line, the frequency decreases, reaches the base line, and then becomes imaginary (in this graph, the negative frequencies actually corresponds to imaginary frequencies of same modulus). The phonon frequency still decreases along the *MR* line and reaches its minimum in the *R* point. This phase is unstable. On the contrary, in part (b), the *Pnma* orthorhombic phase, obtained from condensation of the unstable phonons from *R* and *M*, presents all real positive frequencies, hence this phase is (meta) stable.

Of course even if all ω_σ are real, when large displacements are present, anharmonic effects may be such that another "basin of attraction" is reached, and the structure will feel a force towards that other local minimum of energy. Temperature effects might allow the system to evolve spontaneously from one phase to the other if the energy of the latter is lower. This possibility will be likely only if the barrier of energy between the two structures is sufficiently small, compared to the *kT* temperature factor of the Boltzmann distribution. On the contrary, if the temperature is quite low, no phase transition will take place spontaneously, even if there is a lower-energy structure.

Thus, the knowledge of the full phonon band structure in mineralogy allows either to predict a phase instability, or, on the contrary, to give a positive answer concerning the (meta) stability of a phase.

6. Thermodynamical properties

We will focus on the Helmholtz free energy, the internal energy, the constant-volume specific heat, and the entropy as functions of temperature. Such thermodynamic functions of a solid are determined mostly by the vibrational degrees of freedom of the lattice, since, generally speaking, the electronic degrees of freedom play a noticeable role only for metals at very low temperatures [31]. However, the complete knowledge of the phonon band structure, with sufficient accuracy, is required for the calculation of these thermodynamic functions. The formula presented here neglect all anharmonic effects. For most solids, the harmonic approximation will be accurate for a temperature smaller than a significant fraction of the melting temperature or the temperature of the lowest solid-solid phase transition (e.g. about 500 K for quartz, that undergoes a phase transition above 800 K). On the other hand, the quantum effects are correctly included, unlike in an approach based on the classical dynamics of nuclei.

The above-mentioned thermodynamic functions require summations over phonon eigenstates labeled by the phonon wavevector $\mathbf{q}$ and the phonon mode m. Interestingly, the expressions f to be evaluated at each $\mathbf{q}$ and m depend on $\mathbf{q}$ and m only through the frequency $\omega_{m\mathbf{q}}$. One can then turn $\sum_{m\mathbf{q}} f(\omega_{m\mathbf{q}})$ into a one-dimensional integral $(3N_n) \int_0^{\omega_L} f(\omega)\, g(\omega)\, d\omega$, where N_n is the number of nuclei per unit cell, ω_L is the largest phonon frequency, and $g(\omega)\, d\omega$ is defined to be the fractional number of phonon frequencies in the range between ω and $\omega + d\omega$. The pho-
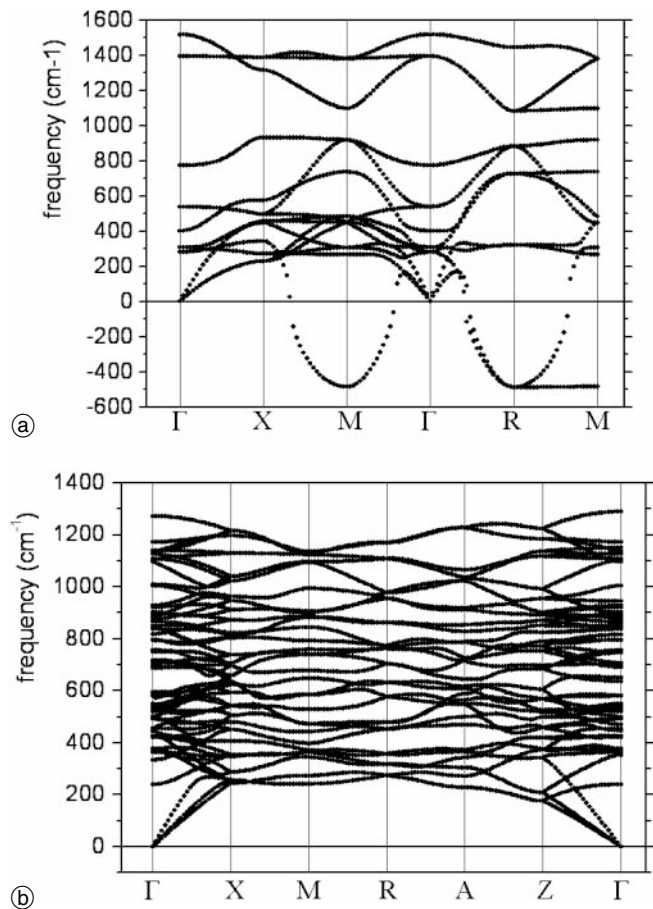
Fig. 3. Phonon dispersion relations for $MgSiO_3$. The ideal cubic phase (**a**) is unstable, while condensations of the unstable phonon modes from *M* and *R* of the cubic structure generate a (meta) stable orthorhombic phase (**b**). The notation of the **q**-wavevectors is: $\Gamma = (0, 0, 0)$; $X = (^1/_2, 0, 0)$, $M = (^1/_2, ^1/_2, 0)$, $R = (^1/_2, ^1/_2, ^1/_2)$, $A = (^1/_2, 0, ^1/_2)$ and $Z = (0, 0, ^1/_2)$.

non density of states $g(\omega)$ can be normalized so that $\int_0^{\omega_L} g(\omega)\,\mathrm{d}\omega = 1$, namely,

$$g(\omega) = \frac{(2\pi)^3}{\Omega_0(3N_n)} \sum_m \int_{BZ} \delta(\omega - \omega_{m\mathbf{q}})\,\mathrm{d}\mathbf{q}\,. \tag{57}$$

Specifically, the phonon contribution to the Helmholtz free energy ΔF, the phonon contribution to the internal energy ΔE, as well as the constant-volume specific heat C_v, and the entropy S, at temperature T, and evaluated for one unit cell, have the following expressions within the harmonic approximation [41], where $x = \dfrac{\hbar\omega}{k_B T}$ and k_B is the Boltzmann constant:

$$\Delta F = (3N_n)\,k_B T \int_0^{\omega_L} \left\{\ln\left(e^x - 1\right) - x/2\right\} g(\omega)\,\mathrm{d}\omega$$

$$\Delta E = (3N_n) \int_0^{\omega_L} \left(\frac{e^x + 1}{e^x - 1}\right)\frac{\hbar\omega}{2}\,g(\omega)\,\mathrm{d}\omega$$

$$C_v = (3N_n)\,k_B \int_0^{\omega_L} \left(\frac{x}{e^{x/2} - e^{-x/2}}\right)^2 g(\omega)\,\mathrm{d}\omega$$

$$S = (3N_n)\,k_B \int_0^{\omega_L} \left[\frac{x\,e^x}{e^x - 1} - \ln\left(e^x - 1\right)\right] g(\omega)\,\mathrm{d}\omega\,.$$

As examples, we apply these formulas to the computation of thermodynamical functions for two polymorphs of silica : quartz and stishovite [9]. In SiO_2-quartz (3 formula unit per primitive cell), each oxygen atom is bonded to two silicon atoms, with a rather open $145°$ angle between the vectors pointing toward these atoms. The silicon atoms are bonded to four oxygen atoms, in a tetrahedral configuration. Thus the quartz lattice is made of tetrahedra, rather rigid, linked by $Si-O-Si$ bonds, that have the ability to rotate. By contrast, in SiO_2-stishovite (2 formula unit per primitive cell), a high-pressure form of SiO_2, the oxygen atoms are three-fold coordinated, and the silicon atoms are six-fold coordinated, with the oxygen and three silicon lying in a plane. This structure, as a whole, is more rigid than the quartz structure, but does not contain a compact building block like the SiO_4 tetrahedron of quartz.

The phonon densities of states of α-quartz and stishovite are presented in Ref. [9] (Fig. 1). These two densities of states are quite different; α-quartz has more complex structure with a very high peak at around $1060\ \mathrm{cm}^{-1}$, a wide gap between 846 and $1038\ \mathrm{cm}^{-1}$, and the largest frequency $1218\ \mathrm{cm}^{-1}$, whereas stishovite has a continuous distribution and the largest frequency $1050\ \mathrm{cm}^{-1}$. α-quartz has a significant density at low frequencies, while stishovite has a low density until the first peak (around $350\ \mathrm{cm}^{-1}$) is reached. On the basis of this phonon frequency analysis, the stishovite lattice could be characterized as more rigid than the α-quartz lattice, as mentioned earlier, if it were not for the presence of the large frequency modes of quartz, beyond $1050\ \mathrm{cm}^{-1}$. The latter
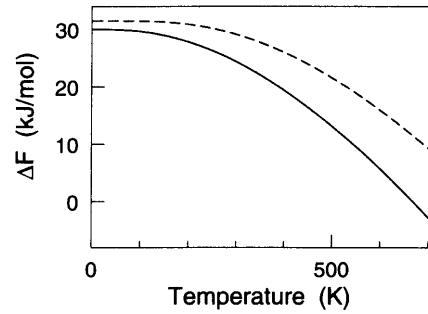
Fig. 4. The phonon contribution to the Helmholtz free energies ΔF of α-quartz (solid line) and stishovite (dashed line). Reprinted from Ref. [9].

modes can be associated with the breathing and distortion of the tetrahedral building blocks SiO_4. Due to the fact that at low temperature more phonon states are available in α-quartz than in stishovite, a difference is expected in the thermodynamic functions.

The temperature-dependent phonon contributions ΔF and ΔE to the Helmholtz free energy F (see Fig. 4) and the internal energy E (see Fig. 5) are calculated from the phonon densities of states [9]. The temperature-dependent ΔE is higher for stishovite between 0 and 200 K and higher for α-quartz above 200 K, whereas ΔF is higher for stishovite at all temperature due to the lower entropy of the more rigid structure of stishovite. The zero-temperature values, ΔF_0 and ΔE_0, do not vanish, due to the zero-point motion. They can be computed:

$$\Delta F_0 = \Delta E_0 = (3N_n) \int_0^{\omega_L} \frac{\hbar\omega}{2}\,g(\omega)\,\mathrm{d}\omega\,. \tag{58}$$

We find $\Delta F_0 = \Delta E_0 = 30.0\ \mathrm{kJ/mol}$ for α-quartz and $31.5\ \mathrm{kJ/mol}$ for stishovite. Note that the harmonic approximation will break down for α-quartz as soon as the temperature approaches 846 K, where a second-order phase transition to β-quartz takes place.

Next, the constant-volume specific heats C_v are calculated and compared to the experimental data from Refs. [42, 43]. The agreement between calculated specific heats and the experimental data is excellent as shown in Fig. 6. The discrepancies between the calculated and experimental specific heat become larger at high temperature as the lattice undergoes thermal expansion due to the anharmonic interactions. Stishovite has lower specific heat than α-quartz at temperature below 480 K and the specific heats of α-quartz and stishovite are very close above 480 K. Also, the two
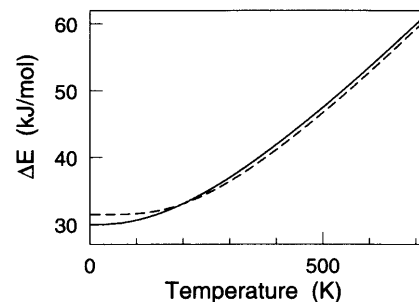
Fig. 5. The phonon contribution to the internal energies ΔE of α-quartz (solid line) and stishovite (dashed line). Reprinted from Ref. [9].
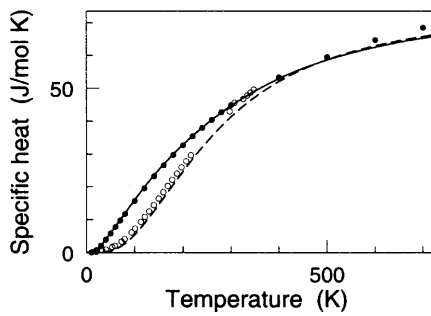
Fig. 6. The constant-volume specific heats of α-quartz (solid line: calculated values; filled circles, experimental data from Ref. [42]) and stishovite (dashed line: calculated values; empty circles, experimental data from Ref. [43]). Reprinted from Ref. [9].
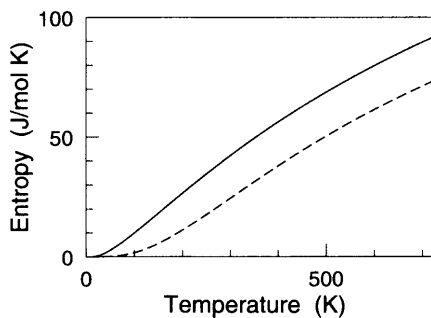
Fig. 7. The entropy of α-quartz (solid line) and stishovite (dashed line). Reprinted from Ref. [9].

specific heats approach at high temperatures the classical asymptotic limit of 74.8 J/mol · K. The entropies are also calculated (see Fig. 7). Stishovite is found to have lower entropy than α-quartz over the entire temperature range, due to its smaller density of states for low frequency modes.

7. The atomic temperature factors

The knowledge of interatomic force constants allows one to compute the atomic temperature factors, which describe the attenuation of X-ray diffraction intensities due to the thermal motion of the atoms. A wealth of information on these atomic temperature factors, gathered by crystallographers, is available.

If the nuclei occupied definite positions in the crystal, the intensity of diffraction would be proportional to the square of the structure factor F defined as $\sum_{\kappa} f_{\kappa} \, e^{2\pi i \mathbf{G} \cdot \tau_{\kappa}}$, where f_{κ} is the scattering amplitude of the atom κ, $\mathbf{G}$ is the scattering wavevector, and τ_{κ} is the position of the nucleus κ. The diffraction condition requires $\mathbf{G}$ to be a reciprocal lattice vector. At finite temperature, the nuclei oscillate around their equilibrium positions and the structure factor is modified as $F(T) = \sum_{\kappa} f_{\kappa} \, e^{-W(\kappa, T)} \, e^{2\pi i \mathbf{G} \cdot \tau_{\kappa}}$ where the atomic temperature factor $e^{-W(\kappa, T)}$ at temperature T is defined [44] as

$$e^{-W(\kappa, T)} = \exp\left(-\frac{1}{2} \sum_{\alpha\beta} B_{\alpha\beta}(\kappa, T) \, G_i G_j\right). \quad (59)$$

The mean-square displacement matrix $B_{\alpha\beta}(\kappa, T)$ is given in terms of "generalized" density of states $g_{\alpha\beta}(\kappa \mid \omega)$ as

Table 2. The thermal parameter β_{ij} of Si and O atoms in α-quartz at room temperature. β_{ij}'s are in Å^2. Ref. [9] is the theoretical prediction. Other data are experimental.

	Atom	β_{11}	β_{22}	β_{33}	β_{12}	β_{13}	β_{23}
Ref. [9]	Si	0.0070	0.0055	0.0054	$\frac{1}{2}\beta_{22}$	$\frac{1}{2}\beta_{23}$	−0.0004
Ref. [79]	Si	0.0045	0.0025	0.0072	$\frac{1}{2}\beta_{22}$	$\frac{1}{2}\beta_{23}$	−0.0002
Ref. [80]	Si	0.0048	0.0027	0.0063	$\frac{1}{2}\beta_{22}$	$\frac{1}{2}\beta_{23}$	0.0004
Ref. [81]	Si	0.0065	0.0054	0.0059	$\frac{1}{2}\beta_{22}$	$\frac{1}{2}\beta_{23}$	−0.0002
Ref. [82]	Si	0.0066	0.0051	0.0060	$\frac{1}{2}\beta_{22}$	$\frac{1}{2}\beta_{23}$	−0.0003
Ref. [83]	Si	0.0085	0.0072	0.0073	$\frac{1}{2}\beta_{22}$	$\frac{1}{2}\beta_{23}$	−0.0002
Ref. [9]	O	0.0155	0.0109	0.0103	0.0090	−0.0033	−0.0042
Ref. [79]	O	0.0131	0.0074	0.0133	0.0078	−0.0037	−0.0049
Ref. [80]	O	0.0128	0.0105	0.0128	0.0069	−0.0035	−0.0044
Ref. [81]	O	0.0163	0.0127	0.0128	0.0097	−0.0027	−0.0043
Ref. [82]	O	0.0156	0.0115	0.0119	0.0092	−0.0029	−0.0046
Ref. [83]	O	0.0174	0.0132	0.0123	0.0097	−0.0029	−0.0041

follows, $\left(x = \dfrac{\hbar\omega}{k_B T}, \text{ and } k_B \text{ is the Boltzmann constant}\right)$:

$$B_{\alpha\beta}(\kappa, T) = \frac{1}{M_\kappa} \int_0^{\omega_L} \frac{\hbar}{2\omega} \left(\frac{e^x + 1}{e^x - 1}\right) g_{\alpha\beta}(\kappa \mid \omega) \, d\omega, \quad (60)$$

with

$$g_{\alpha\beta}(\kappa \mid \omega) = \frac{(2\pi)^3}{\Omega_0} \sum_m \int_{BZ}$$
$$\times \left(M_\kappa U_{m\mathbf{q}}(\kappa\alpha) \, U_{m\mathbf{q}}^*(\kappa\beta)\right) \delta(\omega - \omega_{m\mathbf{q}}) \, d\mathbf{q}.$$

The generalized density of states $g_{\alpha\beta}(\kappa \mid \omega)$ has to be calculated only once for each atom κ and is normalized in such a way that $\int_0^{\omega_L} g_{\alpha\beta}(\kappa \mid \omega) \, d\omega = \delta_{\alpha\beta}$ for each atom κ.

When there is only one kind of atom with sufficient local symmetry, all the $e^{-W(\kappa, T)}$ are identical and $|F(T)|^2 = |F|^2 \, e^{-2W(\kappa, T)}$. In this case, the intensity of diffraction is reduced by a factor of $e^{-2W(\kappa, T)}$, which is usually called the Debye-Waller factor. For two or more kinds of atoms, the relation between $|F|^2$ and $|F(T)|^2$ is not as simple.

As an application, the mean-square displacement matrix elements $B_{\alpha\beta}(\kappa, T)$ for Si and O atoms in α-quartz and stishovite were calculated as a function of temperature [9]. Crystallographers, however, often provide the thermal parameters $\beta_{\alpha\beta}(\kappa)$ (usually at room temperature) which

Table 3. The thermal parameter $\beta_{ij}(\kappa)$ of Si and O atoms in stishovite at room temperature. β_{ij}'s are in Å^2. Ref. [9] is the theoretical prediction. Other data are experimental.

	Atom	β_{11}	β_{22}	β_{33}	β_{12}	β_{13}	β_{23}
Ref. [9]	Si	0.00228	β_{11}	0.00177	0.00007	0	0
Ref. [84]	Si	0.00253	β_{11}	0.00196	0.00014	0	0
Ref. [85]	Si	0.00236	β_{11}	0.00178	0.00016	0	0
Ref. [9]	O	0.00301	β_{11}	0.00238	−0.00082	0	0
Ref. [84]	O	0.00327	β_{11}	0.00248	−0.00095	0	0
Ref. [85]	O	0.00308	β_{11}	0.00231	−0.00084	0	0
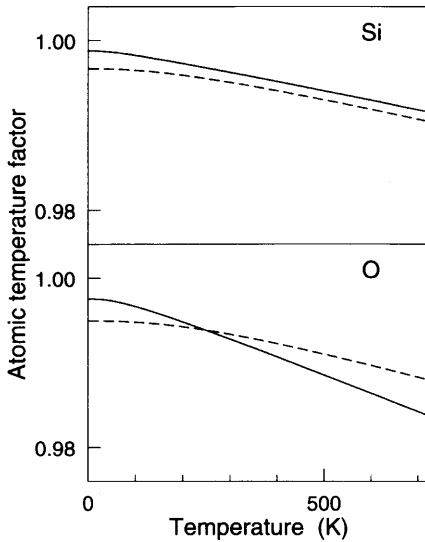
Fig. 8. The atomic temperature factors of Si and O atoms in α-quartz (solid line) and stishovite (dashed line) for the diffraction with scattering vector $\mathbf{G} = (2\pi/c)\,\hat{\mathbf{z}}$. Reprinted from Ref. [9].

are the mean-square displacements of the atom κ along the *crystal* axes α and β. Therefore, one has to convert the mean-square displacement matrix $B_{\alpha\beta}(\kappa, T)$ into the thermal parameters $\beta_{ij}(\kappa)$ for comparison. Due to the symmetry of the crystal structure, $\beta_{22}(\text{Si}) = 2\beta_{12}(\text{Si})$ and $\beta_{23}(\text{Si}) = 2\beta_{13}(\text{Si})$ in α-quartz, and $\beta_{11}(\kappa) = \beta_{22}(\kappa)$ and $\beta_{13}(\kappa) = \beta_{23}(\kappa) = 0$ for $\kappa = \text{Si}$ or O in stishovite. Experimental values, obtained from analysis of raw data through model calculations, show large discrepancies between each others. Calculated values show reasonable agreement with these results (see Tables 2 and 3). The sole large systematic discrepancy, over 10%, is found for the β_{33} element in α-quartz. This discrepancy could be due to the anharmonicity of the interatomic potential. Experimental uncertainties likely preclude the observation of this effect for the other components of the β tensor in α-quartz, while stishovite is a less anharmonic material than α-quartz. The typical mean-square displacements of Si and O atoms in stishovite are rather similar (between 0.00177 and 0.00301 Å^2), while the mean-square displacement of the Si atoms in α-quartz is roughly three times larger than this value (0.0054 and 0.0070 Å^2), and the β_{11} component of the O atoms reaches up to 0.0155 Å^2. The smaller displacements in stishovite are a consequence of the rigidity of its lattice. The atomic temperature factors $e^{-W(\kappa, T)}$ are also calculated for the diffraction with scattering vector $\mathbf{G} = (2\pi/c)\,\hat{\mathbf{z}}$ (see Fig. 8). $e^{-W(\kappa, T)}$ is not 1 even at 0 K due to the zero-point motion. The O atoms in α-quartz, having large mean-square displacements, show larger change in the atomic temperature factor as a function of temperature than the Si atoms in α-quartz and the Si or O atoms in stishovite.

8. Discussion and perspectives

In the present review, we have focused on different properties of minerals, linked to lattice dynamics, that can be obtained from first principles, using the density-functional

perturbation theory. We have presented the theory, as well as selected examples, for: (i) the computation of phonons at the Brillouin-zone center, observed in infra-red and Raman experiments; (ii) the computation of phonon band structures allowing to assert the stability/instability of a phase; (iii) thermodynamical properties (specific heat, internal energy, free energy, entropy; (iv) atomic temperature factors. Although we do not intend to be exhaustive, the reader will find further information and applications of this formalism, at the level of lattice-dynamical properties, in Refs. [45–59].

We have only focused on the specific properties linked to lattice vibrations. Density-functional perturbation theory is also able to treat, at the linear-response level, perturbations that modify the unit cell parameters. Taking account mixed perturbations, such perturbations allow to compute the elastic tensor and the piezoelectric tensor. However, applications of this possibility have been scarce until now, see e.g. Refs. [60–63].

At the non-linear level [4, 8], combining the first-order wavefunctions from phonon, electric field and strain type perturbations, the scope of DFPT is rather large, and allows, directly or indirectly, the computation of the thermal expansion, non-linear elastic constants, non-linear dielectric response, Raman scattering efficiencies, phonon lifetimes, Raman linewidths, etc. Some of these properties are already available in different softwares, while other still awaits to be coded. Actually, finite differences can be used on top of DFPT to derive non-linear properties that have not yet been implemented. As examples of the use of DFPT for the prediction of non-linear properties, the users might consult Refs. [33, 64–71].

Although the DFPT is the most powerful approach to the dynamical properties of minerals, it is possible to obtain interatomic force constants also by finite difference of total energy and force calculations, in large supercells. If one uses the same basis set for the representation of the electronic wavefunctions, with the same relevant parameters, the final results from both methods should be strictly identical (only the numerical efficiency will be different). By this technique, phonon band structures have been obtained by interpolation for many different minerals. As examples of such studies, we have selected Refs. [72–76].

References

[1] Hohenberg, P.; Kohn, W.: Inhomogeneous electron gas. Phys. Rev. **136** (1964) B864-B871.

[2] Kohn, W.; Sham, L. J.: Self-consistent equations including exchange and correlation effects. Phys. Rev. **140** (1965) A1133–A1138.

[3] Baroni, S.; Giannozzi, P.; Testa, A.: Green's-function approach to linear response in solids. Phys. Rev. Lett. **58** (1987) 1861–1864.

[4] Gonze, X.; Vigneron, J.-P.: Density-functional approach to non-linear-response coefficients of solids. Phys. Rev. B**49** (1989) 13120–13128.

[5] Gonze, X.; Allan, D. C.; Teter, M. P.: Dielectric tensor, effective charges and phonon in α-quartz by variational density-functional perturbation theory. Phys. Rev. Lett. **68** (1992) 3603–3606.

[6] Savrasov, S. Yu.: Linear response calculations of lattice dynamics using muffin-tin basis sets. Phys. Rev. Lett. **69** (1992) 2819–2822.

[7] Gonze, X.; Charlier, J.-C.; Allan, D. C.; Teter, M. P.: Inter-atomic force constants from first principles: The case of α-quartz. Phys. Rev. B**50** (1994) 13035–13038.

[8] Gonze, X.: Adiabatic density functional perturbation theory. Phys. Rev. A**52** (1995) 1096–1114.

[9] Lee, C.; Gonze, X.: Ab initio calculation of the thermodynamical properties and atomic temperature factors of SiO_2 α-quartz and stishovite. Phys. Rev. B**51** (1995) 8610–8613.

[10] De Gironcoli, S.: Lattice dynamics of metals from density-functional perturbation theory. Phys. Rev. B**51** (1995) 6773–6776.

[11] Gonze, X.: First-principle responses of solids to atomic displacements and homogeneous electric fields: implementation of a conjugate-gradient algorithm. Phys. Rev. B**55** (1997) 10337–10354.

[12] Gonze, X.; Lee C.: Dynamical matrices, Born effective charges, dielectric permittivity tensors, and interatomic force constants from density-functional perturbation theory. Phys. Rev. B**55** (1997) 10355–10368.

[13] Putrino, A.; Sebastiani, D.; Parrinello, M.: Generalized variational density functional perturbation theory. J. Chem. Phys. **113** (2000) 7102–7109.

[14] Baroni, S.; de Gironcoli, S.; Dal Corso, A.; Giannozzi, P.: Phonons and related crystal properties from density-functional perturbation theory. Rev. Mod. Phys. **73** (2001) 515–562.

[15] Scandolo, S.; Giannozzi, P.; Cavazzoni, C.; de Gironcoli, S.; Pasquarello, A.; Baroni, S.: First-principles codes for computational crystallography in the Quantum-ESPRESSO package. Z. Kristallogr. **220** (2005) 574–579.

[16] http://www.pwscf.org

[17] Gonze, X.; Rignanese, G.-M.; Verstraete, M.; Beuken, J.-M.; Pouillon, Y.; Caracas, R.; Jollet, F.; Torrent, M.; Zérah, G.; Mikami, M.; Ghosez, Ph.; Veithen, M.; Raty, J.-Y.; Olevano, V.; Bruneval, F.; Reining, L.; Godby, R.; Onida, G.; Hamann, D. R.; Allan, D. C.: A brief introduction to the ABINIT software package. Z. Kristallogr. **220** (2005) 558–562.

[18] http://www.abinit.org

[19] Gonze, X.; Beuken, J.-M.; Caracas, R.; Detraux, F.; Fuchs, M.; Rignanese, G.-M.; Sindic, L.; Verstraete, M.; Zerah, G.; Jollet, F.; Torrent, M.; Roy, A.; Mikami, M.; Ghosez, Ph.; Raty, J.-Y.; Allan, D. C.: First-principle computation of material properties: the ABINIT software project. Comput. Materials Science **25** (2002) 478–492.

[20] Hutter, J.; Iannuzzi, M.: CPMD: Car-Parrinello Molecular Dynamics. Z. Kristallogr. **220** (2005) 549–551.

[21] http://www.cpmd.org

[22] Savrasov, S. Y.: Program LMTART for electronic structure calculations. Z. Kristallogr. **220** (2005) 555–557.

[23] http://www.fkf.mpg.de/andersen/docs/interest.html

[24] Rignanese, G.-M.; Detraux, F.; Gonze, X.; Bongiorno, A.; Pasquarello, A.: Dielectric constants of Zr silicates: a first-principles study. Phys. Rev. Lett. **89** (2002) 117601: 1–4.

[25] Lee, C.; Gonze, X.: The pressure-induced ferroelastic phase transition of SiO_2-stishovite. J. Phys.: Condens. Matter **7** (1995) 3693–3698.

[26] Ghosez, Ph.; Michenaud, J.-P.; Gonze, X.: Dynamical atomic charges: the case of ABO_3 compounds. Phys. Rev. B**58** (1998) 6224–6240.

[27] Caracas, R.; Gonze, X.: First-principle study of materials involved in incommensurate transitions. Z. Kristallogr. (2005) 511–520.

[28] In general, the perturbation could also directly affect the kinetic operator, as well as the exchange-correlation functional or even the Hartree functional. These effects are not considered here. See Ref. [11] for further information.

[29] Sternheimer, R. M.: Electronic Polarizabilities of Ions from the Hartree-Fock Wave Functions. Phys. Rev. **96** (1954) 951–968.

[30] Altmann, S. L.: Band theory of solids: an introduction from the point of view of symmetry. Oxford University Press, Oxford (1991).

[31] Landau, L.; Lifschits, E.: Electrodynamics of Continuous Media. Pergamon Press, (1960).

[32] Pick, R. M.; Cohen, H.; Martin, R. M.: Microscopic Theory of Force Constants in the Adiabatic Approximation. Phys. Rev. B**1** (1970) 910–920.

[33] Veithen, M.; Gonze, X.; Ghosez, Ph.: Non-linear optical susceptibilities, Raman efficiencies and electrooptic tensors from first-principles density functional perturbation theory. Phys. Rev. B**71** (2005) 125107.

[34] There are conflicting definitions for associated quantities, like the mode-effective charges and oscillator strengths. In order to avoid further confusion, we have uses mode polarities in all our formulas, since these are not subject to such conflicting definitions.

[35] Ghosez, Ph.: First-principles study of the dielectric and dynamical properties of barium titanate. Ph.D. thesis, Université Catholique de Louvain (1997), unpublished.

[36] Laabidi, K.; Fontana, M. D.; Jannot, B.: Underdamped soft phonon in orthorhombic $BaTiO_3$. Solid State Comm. **76** (1990) 765.

[37] Dawson, P.; Hargreave, M. M.; Wilkinson, G. R.: The vibrational spectrum of zircon ($ZrSiO_4$). J. Phys. C: Solid State Phys. **4** (1971) 240–256.

[38] Rignanese, G.-M.; Gonze, X.; Pasquarello, A.: First-principles study of structural, electronic, dynamical, and dielectric properties of zircon. Phys. Rev. B**63** (2001) 104305: 1–7.

[39] Gervais, F.; Piriou, B.; Cabannes, F.: Anharmonicity in silicate crystals: Temperature dependence of A_u type vibrational modes in $ZrSiO_4$ and $LiAlSi_2O_6$. J. Phys. Chem. Solids **34** (1973) 1785–1796.

[40] Pecharromán, C.; Ocaña, M.; Tartaj, P.; Serna, C. J.: Infrared Optical-Properties of Zircon. Mater. Res. Bull. **29** (1994) 417–426.

[41] Maradudin, A. A.; Montroll, E. W.; Weiss, G. H.; Ipatova, I. P.: Theory of lattice dynamics in the harmonic approximation in Solid State Physics (Eds. H. E. Ehrenreich; F. Seitz; D. Turnbull). Academic Press, New York, (1971), 2nd ed. Chap. 4.

[42] Lord, R. C.; Morrow, J. C.: Calculation of the heat capacity of alpha quartz and vitreous silica from spectroscopic data. J. Chem. Phys. **26** (1957) 230.

[43] Holm, J. L.; Kleppa, O. J.; Westrum, E. F. Jr.: Thermodynamics of polymorphic transformations in silica. Thermal properties from 5 to 1070 K and pressure-temperature stability fields for coesite and stishovite. Geochim. Cosmochim. Acta **31** (1967) 2289.

[44] Willis, B. T. M.; Pryor, A. W.: Thermal vibrations in crystallography. Cambridge University Press, (1975).

[45] Giannozzi, P.; de Gironcoli, S.; Pavone, P.; Baroni, S.: Ab initio calculation of phonon dispersions in semiconductors. Phys. Rev. B**43** (1991) 7231–7242.

[46] Nardelli, M. B.; Baroni, S.; Giannozzi, P.: Phonon softening and high-pressure low-symmetry phases of cesium iodide. Phys. Rev. Lett. **69** (1992) 1069–1072.

[47] Vast, N.; Baroni, S.; Zerah, G.; Besson, J. M.; Polian, A.; Grimsditch, M.; Chervin, J. C.: Lattice Dynamics of Icosahedral α-Boron under Pressure. Phys. Rev. Lett. **78** (1997) 693–696.

[48] Saitta, A. M.; Alfe, D.; de Gironcoli, S.; Baroni, S.: Phonon Softening and Elastic Instabilities in the Cubic-to-Orthorhombic Structural Transition of CsH. Phys. Rev. Lett. **78** (1997) 4958–4961.

[49] Ghosez, Ph.; Cockayne, E.; Waghmare, U. V.; Rabe, K. M.: Lattice dynamics of $BaTiO_3$, $PbTiO_3$, and $PbZrO_3$: A comparative first-principles study. Phys. Rev. B**60** (1999) 836–843.

[50] Lazzari, R.; Vast, N.; Besson, J. M.; Baroni, S.; Dal Corso, A.: Atomic Structure and Vibrational Properties of Icosahedral B_4C Boron Carbide. Phys. Rev. Lett. **83** (1999) 3230–3233.

[51] Wang, C.-Z.; Yu, R.; Krakauer, H.: First-principles calculations of phonon dispersion and lattice dynamics in La_2CuO_4. Phys. Rev. B**59** (1999) 9278−9284.

[52] Dal Corso, A.; and S. de Gironcoli, S.: Ab initio phonon dispersions of Fe and Ni. Phys. Rev. B **62** (2000) 273−277.

[53] Veithen, M.; Ghosez, Ph.: First-principles study of the dielectric and dynamical properties of lithium niobate. Phys. Rev. B**65** (2002) 214302: 1−12.

[54] Bungaro, C.; Rabe, K. M.; Dal Corso, A.: First-principles study of lattice instabilities in ferromagnetic Ni_2MnGa. Phys. Rev. B**68** (2003) 134104: 1−9.

[55] Oganov, A. R.; Gillan, M. J.; Price, G. D.: Ab initio lattice dynamics and structural stability of MgO. J. Chem. Phys. **118** (2003) 10174−10182.

[56] Clatterbuck, D. M.; Krenn, C. R.; Cohen, M. L.; Morris, J. W.: Phonon instabilities and the ideal strength of aluminum. Phys. Rev. Lett. **91** (2003) 135501.

[57] Verstraete, M.; Gonze, X.: First-principles calculation of the electronic, dielectric, and dynamical properties of CaF_2. Phys. Rev. B**68** (2003) 195123.

[58] Caracas, R.; Gonze, X.: Ab initio determination of the ground-state properties of $Ca_2MgSi_2O_7$ akermanite. Phys. Rev. B**68** (2003) 184102.

[59] Serrano, J.; Romero, A. H.; Manjon, F. J.; Lauck, R; Cardona, M; Rubio, A.: Pressure dependence of the lattice dynamics of ZnO: An ab initio approach. Phys. Rev. B**69** (2004) 094306.

[60] Baroni, S.; Giannozzi, P.; Testa, A.: Elastic Constants of Crystals from Linear-Response Theory. Phys. Rev. Lett. **59** (1987) 2662−2665.

[61] de Gironcoli, S.; Baroni, S.; Resta, R.: Piezoelectric properties of III−V semiconductors from first-principles linear-response theory. Phys. Rev. Lett. **62** (1989) 2853−2856.

[62] Dal Corso, A.; Resta, R.; Baroni, S.: Nonlinear piezoelectricity in CdTe. Phys. Rev. B**47** (1993) 16252−16256.

[63] Hamann, D. R.; Wu, X.; Rabe, K. M.; Vanderbilt, D.: Metric tensor formulation of strain in density-functional perturbation theory. Phys. Rev. B**71** (2005) 035117.

[64] Dal Corso, A.; Mauri, F.: Wannier and Bloch orbital computation of the nonlinear susceptibility. Phys. Rev. B**50** (1994) 5756−5759.

[65] Debernardi, A.; Baroni, S.; Molinari, E.: Anharmonic Phonon Lifetimes in Semiconductors from Density-Functional Perturbation Theory. Phys. Rev. Lett. **75** (1995) 1819−1822.

[66] Ulrich, C.; Anastassakis, E.; Syassen, K.; Debernardi, A.; Cardona, M.: Lifetime of Phonons in Semiconductors under Pressure. Phys. Rev. Lett. **78** (1997) 1283−1286.

[67] Umari, P.; Pasquarello, A.; Dal Corso, A.: Raman scattering intensities in α-quartz: A first-principles investigation. Phys. Rev. B**63** (2001) 094305: 1−9.

[68] Debernardi, A.; Alouani, M.; Dreyssé, H.: Ab initio thermodynamics of metals: Al and W. Phys. Rev. B**63** (2001) 064305: 1−7.

[69] Detraux, F.; Gonze, X.: Photoelasticity of α-quartz from first-principles. Phys. Rev. B**63** (2001) 115118: 1−7.

[70] Deinzer, G.; Strauch, D.: Raman tensor calculated from the $2n+1$ theorem in density-functional theory. Phys. Rev. B**66** (2002) 100301: 1−3.

[71] Deinzer, G.; Strauch, D.: Two-phonon infrared absorption spectra of germanium and silicon calculated from first principles. Phys. Rev. B**69** (2004) 045205: 1−6.

[72] Wei, S. and M. Y. Chou, M. Y.: Ab initio calculation of force constants and full phonon dispersions. Phys. Rev. Lett. **69** (1992) 2799−2802.

[73] Parlinski, K.; Li, Z. Q.; Kawazoe, Y.: First-Principles Determination of the Soft Mode in Cubic ZrO. Phys. Rev. Lett. **78** (1997) 4063−4066; see also Refs. [77] and [78].

[74] Parlinski, K.; Li, Z. Q.; Kawazoe, Y.: Ab initio calculations of phonons in $LiNbO_3$. Phys. Rev. B**61** (2000) 272−278.

[75] Parlinski, K.; Parlinska-Wojtan, M.: Lattice dynamics of NiTi austenite, martensite, and R phase. Phys. Rev. B**66** (2002) 064307: 1−8.

[76] Lodziana, Z.; Parlinski, K.: Dynamical stability of the alpha and theta phases of alumina. Phys. Rev. B**67** (2003) 174106: 1−7.

[77] Detraux, F.; Ghosez, Ph.; Gonze, X.: Long-range Coulomb interaction in ZrO_2. Phys. Rev. Lett. **81** (1998) 3297.

[78] Parlinski, K.; Li, Z. Q.; Kawazoe, Y.: Parlinski, Li, and Kawazoe Reply. Phys. Rev. Lett. **81** (1998) 3298.

[79] Young, R. A.; Post, B.: Electron density and thermal effects in alpha quartz. Acta Crystallogr. **15** (1992) 337.

[80] Smith, G. S.; Alexander, L. E.: Refinement of the atomic parameters of α-quartz. Acta Crystallogr. **16** (1963) 462.

[81] Zachariasen, W. H.; Plettinger, H. A.: Extinction in quartz. Acta Crystallogr. **18** (1965) 710.

[82] Le Page, Y.; Donnay, G.: Refinement of the crystal structure of low-quartz. Acta Crystallogr. B**32** (1976) 2456.

[83] Levien, L.; Prewitt, C.T.; Weidner, D. J.: Structure and elastic properties of quartz at pressure. Am. Mineral. **65** (1980) 920.

[84] Hill, R. J.; Newton, M. D.; Gibbs, G. V.: A crystal chemical study of stishovite. J. Solid State Chem. **47** (1983) 185.

[85] Spackman, M. A.; Hill, R. J.; Gibbs, G. V.: Exploration of structure and bonding in stishovite with Fourier and pseudoatom refinement methods using single crystal and power X-ray diffraction data. Phys. Chem. Minerals **14** (1987) 139.

[86] Warren, J. L.; Yarnell, J. L.; Dolling, G.; Cowley, R. A.: Lattice Dynamics of Diamond. Phys. Rev. **158** (1967) 805−808.

[87] Burkel, E.: Inelastic Scattering of X Rays with Very High Energy Resolution. Vol. 125 of Springer Tracts in Modern Physics. Springer, Berlin, (1991) (especially pp. 61−64).